Available online at www.sciencedirect.com
ScienceDirect
International Journal of Multiphase Flow 33 (2007) 849–872
International Journal of Multiphase Flow
www.elsevier.com/locate/ijmulflow

Experimental estimation of particle flow fluctuations in dense unsteady two-phase flow using phase Doppler anemometry

Tobias Bergenblock [a,*], Fabrice Onofri [b], Bo Leckner [a], Lounès Tadrist [b]

[a] Chalmers University of Technology, Department of Energy Conversion, SE-412 96 Göteborg, Sweden
[b] IUSTI-CNRS, University of Provence, Technopole de Chateau Gombert, 5, rue Enrico Fermi, 13453 Marseille Cedex 13, France

Received 22 April 2006; received in revised form 18 February 2007

Abstract

A recently proposed and successfully validated post-processing algorithm is extended to treat particle data obtained by a phase Doppler anemometer (PDA) in dense, fluctuating, low-speed, two-phase flow. In such a flow, Doppler signals may be noisy and split, since particles have long residence times in the measurement volume. A novel time average based on the measured burst lengths is proposed to estimate the cross-sectional area of the measurement volume. This time average accounts for the possible split of a noisy Doppler burst, and it provides a more general description of the measurement volume than the conventional ensemble average. The extended post-processing algorithm was tested on experimental time series obtained in a circulating fluidized bed and the algorithm was compared to conventional treatment of the particle data by a commercial PDA processor. The conventional processing strongly overestimates the vertical mass flux integrated over the cross-section. In contrast, time-mean and fluctuations of mass flux, particle volume concentration, and particle velocity are reliably estimated employing the proposed algorithm, with continuity check parameters in succeeding particle data, as well as with a particle velocity filter to estimate the size of the probe volume, applying a two-component PDA in a three-dimensional flow.

Keywords: Phase Doppler anemometry; Two-phase flow; Particle data averaging; Circulating fluidized bed; Particle flow measurements

1. Introduction

The aim of this work is to improve the estimation of density and velocity fluctuations in the local particle flow of a low-speed two-phase flow having a wide velocity distribution (but being statistically steady). In principle, a phase Doppler anemometer (PDA) enables such an estimation, provided that the particles are spherical and homogeneous, and that the optical thickness of the disperse flow is not too high (i.e. to avoid multiple

* Corresponding author. Tel.: +46 31 772 1000; fax: +46 31 772 3592.
E-mail address: tobias.bergenblock@xdin.com (T. Bergenblock).

0301-9322/$ - see front matter © 2007 Elsevier Ltd. All rights reserved.
doi:10.1016/j.ijmultiphaseflow.2007.02.004

scattering effects, Onofri et al., 1999). Nevertheless, in fluctuating low-speed flows more fast than slow particles will be detected by a PDA. This leads to a sampling bias; the so-called 'velocity bias' (McLaughlin and Tiederman, 1973; Buchhave et al., 1979). The particle data produced by the PDA need to be corrected for this velocity bias to estimate time-moments and spectral properties of intensive flow variables. Furthermore, the local concentration and velocity of particles may be correlated (the particles may flow in clusters) causing additional bias, and this also requires attention. These two cases of bias have generally not been considered in work on unsteady two-phase flow, such as that related to fluidized bed (Levy and Lockwood, 1983; Hamdullahpur and Mackay, 1986; Berkelmann and Renz, 1991; Yang et al., 1992; Wang et al., 1993; Zhang and Arastoopour, 1995; Samuelsberg and Hjertager, 1996; Werther et al., 1996; van den Moortel et al., 1997; van den Moortel et al., 1998; Mathiesen et al., 2000; Ibsen et al., 2001, 2004). Furthermore, the measurement area and volume of the PDA probe may depend on diameter d and direction γ of the sampled particle (γ is the angle between the velocity vector of the particle, **u**, and the main flow direction, x, as shown in Fig. 1).

In optically dense flows, particles located near the measurement volume $V_{(d,\gamma)}$ may attenuate the laser beams or affect the light scattered in the direction of the PDA detectors. In this work, the optical path consists of two parts: (i) from the emitting laser to the measured particle, and (ii) from the measured particle to the detector. The optical thickness of the path may yield noisy Doppler bursts and burst splitting (van den Moortel et al., 1997). For such a split burst, originating from the passage of a particle through $V_{(d,\gamma)}$, the burst can be interpreted by the signal processor of the PDA as passages of multiple particles with short residence times. Such a difficulty is illustrated in Fig. 2, by the temporal evolution of the characteristics of various Doppler signals analyzed with a sliding cross-spectral correlation algorithm. Fig. 2 shows processing of normal Doppler signals (1) as well as of non-ideal (noisy) Doppler signals (2) with oscillating signal-to-noise ratio and phase ratio (i.e. the estimated particle diameters are inaccurate). The non-ideal Doppler bursts could result from classical difficulties, such as trajectory and slit effects (Sankar et al., 1992; Gréhan et al., 1993; Albrecht et al., 2003), but also from burst splitting and perturbations of fringes, which may occur in dense flow. The distance between the probe volume and the particles blocking the laser beams or the scattered light is important. If this distance is small, distortion of the fringes is likely to occur, possibly leading to failure of validation of detected particles. In contrast, a large distance may yield valid particles, and by employing a burst length procedure an estimation is possible of the reduced size of the probe volume caused by the low light intensity.

Another difficulty related to high particle number density in the low-speed flow (where the inter-particle spacing is small and/or the residence time Δt_i of a particle in the measurement volume $V_{(d,\gamma)}$ is long) is the high probability of simultaneous presence of several particles in the measurement volume. This invalidates measurements (Edwards and Marx, 1992). Roisman and Tropea (2001) proposed a method based on Poisson statistics to correct for the influence of particle number density. Unfortunately, Poisson statistics cannot be applied to correlated data (such as encountered in clusters of particles). Thus, particles in dense groups may be wrongly measured and even missed completely. All difficulties mentioned affect the accuracy of

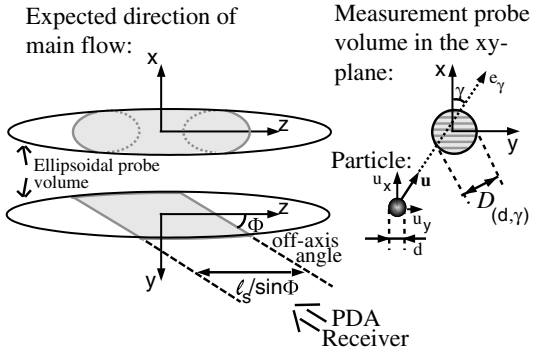

Fig. 1. PDA probe volume (not to scale) and the optical coordinate system. Areas of possible particle detection are shown in gray.

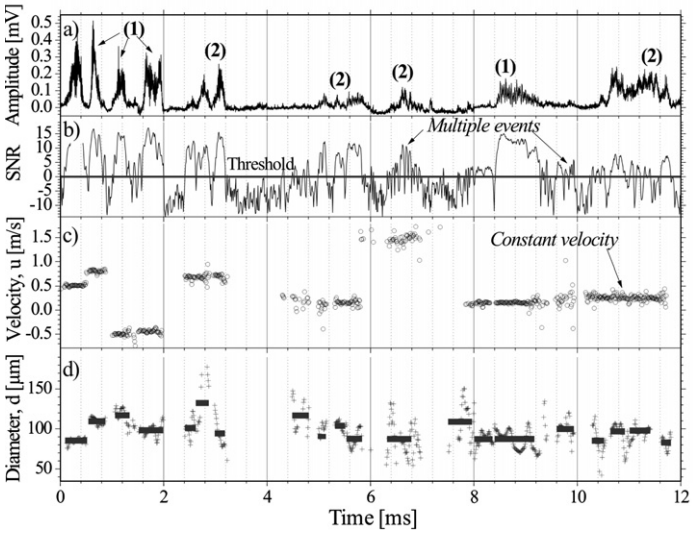

Fig. 2. Illustration of signal processing of experimental Doppler bursts detected in dense particle flow. Amplitude and signal-to-noise ratio (SNR) of burst signals, estimated particle velocity and diameter are shown in: (a), (b), (c) and (d), respectively. Bursts of type (1) are likely to be produced by single particles, whereas bursts of type (2) have oscillating SNR and/or phase ratio (i.e. estimated particle diameters fluctuate) and appear to be split.

PDA measurements in unsteady two-phase flow and need to be considered in order to estimate fluctuations in low-speed particle flow under optically dense conditions.

Recently, a novel PDA data post-processing algorithm was proposed by Bergenblock et al. (2006) to estimate fluctuations in intensive variables (e.g. particle velocity, concentration) of particles detected in statistically steady-state, low-speed, fluctuating flow. The algorithm accounts for high-velocity sampling bias, for possible correlation between velocity and concentration of particles, and performs mass-weighting of intensive flow variables. It was successfully validated by numerical simulation, adopting an Eulerian–Lagrangian approach. To estimate fluctuations in a particle-flow variable, a constant local averaging time Δt_{meso} was applied on the PDA data (van de Wall and Soo, 1994; Hardalupas and Horender, 2001; Bergenblock et al., 2006) to analyze the variable in terms of particle groups on a meso-scale (an intermediate scale between the scales associated with particles and particle clusters, subscript meso). The velocities recorded within Δt_{meso} should be correlated, which they are in clustering flows, so that the introduction of Δt_{meso} does not result in excessive correlation in the estimate (e.g. integral time scale) of the particle velocity. In addition, the length scale of the group should be at least one order of magnitude larger than the particle diameter. The variance of particle volume concentration decreases with larger Δt_{meso}, whereas the integral time-scale increases. The optimum Δt_{meso} is obtained at the point where the integral time scale of the variable equals Δt_{meso} (Bergenblock et al., 2006). Time-mean and fluctuations (expressed by second order time-moments, power spectra, and integral time-scales) of the variables were shown to be correctly estimated. This approach, using a local averaging time on the PDA data, allows a comparison of such averaged data with results obtained from numerical simulations of the particle phase, adopting an Eulerian approach. Time-mean and time-RMS of particle velocity were estimated with a maximum error of less than 2% (of the numerically simulated values averaged over a control volume (CV) much larger than the PDA volume) and the corresponding error for particle volume concentration was 9% due to the rather large average particle concentration (0.0011 [–]), which resulted in presence of multiple particles in the PDA volume. The errors of using the ensemble mean and RMS values of particle velocity were much higher: 35% and 44% (compared to the numerically simulated values over CV).

In Section 2, this previously introduced algorithm is extended to also treat particle data obtained in flows with rather high optical thickness, resulting in burst splitting. This is accomplished by adopting the post-processing algorithm of van den Moortel et al. (1997) and by replacing the ensemble average of the measured

burst length l (Saffman, 1987) with an estimated time-average diameter of the measurement area and volume. Section 3 presents an application of the extended algorithm to a gas/solids flow (unsteady) in a circulating fluidized bed (CFB), with a, relatively seen, high average volume concentration of particles and with wide distributions of particle velocity and diameter. A global mass balance is performed over the cross-section of the riser and the cyclone leg of the CFB to experimentally verify the algorithm in terms of time-average mass flux, see Sections 3 and 4. Finally, fluctuations in particle flow are estimated in Section 4.

2. Derivation of time-moments and probe-volume characteristics

2.1. Time-moments

The volume of the measurement probe $V_{(d,\gamma)}$ of a phase Doppler anemometer (PDA) (indicated in Fig. 1) varies with each sampled particle of the disperse phase in a polydisperse, fluctuating two-phase flow. An ensemble average of the sampled PDA data (velocity, diameter, transit time) will be biased and not representative of the true time-average in flows with fluctuating velocity (but statistically steady), since: (i) there is a higher probability to sample particles with high than with low velocity, (ii) the local particle concentration and velocity may be correlated (e.g. in clusters of particles), and (iii) the measurement volume depends on the size and direction of the measured particle. Considering these three items, the average concentration over a time T of an intensive property, q_P, was derived on a micro scale (similar to the particle size) by Bergenblock et al. (2006) as

$$q_{P\text{-micro}} = \frac{1}{T}\int_0^T \left(\frac{1}{\rho_s V_{(d,\gamma)}} \int_{V_{(d,\gamma)}} \frac{P}{V_s}\,\mathrm{d}V \right) \mathrm{d}t \approx \frac{1}{T}\sum_{i=1}^{K_n} \frac{P_i \Delta t_i}{\rho_s V_{(d,\gamma),i}}, \tag{1}$$

where Δt_i is the transit time in the measurement volume of the ith particle in the measured time series (containing K_n particles of the same material density, ρ_s. In Eq. (1) the extensive mass-based equivalence of q_P is P (V_s is solid volume), and each value of the extensive property P is made intensive by employing an extensive average (i.e. an average over $V_{(d,\gamma)}$) to account for the influence of particle diameter and path angle (d,γ). Note that, if P is particle mass, the corresponding intensive property q_P is particle volume concentration (usually denoted c_v). The transformation of Eq. (1) from continuous to discrete form introduces measurement errors in optically dense flow (in decreasing order): (i) the particle residence time Δt_i, (ii) the size of the measurement volume $V_{(d,\gamma),i}$, and (iii) the particle diameter (to determine P_i). In fact Δt_i may be very inaccurate under optically dense conditions and Eq. (1) should be modified to avoid Δt_i.

For high-speed flows, Eq. (1) can be simplified to

$$q_{P\text{-micro}} \approx \frac{1}{T}\sum_{i=1}^{K_n} \frac{P_i \Delta t_i}{\rho_s V_{(d,\gamma),i}} \approx \frac{1}{T}\sum_{i=1}^{K_n} \frac{P_i}{\rho_s A_{(d,\gamma),i} |\mathbf{u}_i|}, \tag{2}$$

in which $A_{(d,\gamma),i}$ is the cross-sectional area of the measurement volume, normal to the velocity vector of particle i. The residence time Δt_i in Eq. (2) is cancelled out since $V_{(d,\gamma),i} = A_{(d,\gamma),i}|\mathbf{u}|_i \Delta t_i$. This cancellation is fortunate, because Δt_i is subject to noise in optically dense applications. Eqs. (1) and (2) are equal to the equations found in literature (e.g. Roisman and Tropea, 2001) for high-speed applications. In fluctuating low-speed flows, particle velocities near zero may occur, and these can not be dealt with by Eq. (2). Therefore, the equation was converted by an approach that employs a meso-scale (subscript meso) averaging time Δt_{meso}, chosen according to the integral time scale of fluctuations (defined below) in the variable of interest, capable of estimating time-moments of the property q_P in such low-speed flows. The meso-scale averaging, applied on a particle group j with $K_j - K_{j-1}$ particles (where index j denotes succeeding particle groups and K_{j-1} is the number of particles prior to Group j in the time series), filters out the particle velocities near zero in the group, if the group has an average velocity deviating from zero. This filtering reduces the occurrence of division by a velocity near zero. There is no restriction on the number of particles in a particle group, except if the integral time scale of fluctuations of the variable under consideration is unknown. In such a case, the average number of particles in a group should be large enough (at least in the order of 10 particles) to make an estimation of the integral time

scale possible. An absolute value of the velocity vector associated with Group j is estimated as a mass-weighted ensemble average of the velocities of $K_j - K_{j-1}$ particles,

$$|\mathbf{u}_{\text{meso},j}| = \left| \sum_{i=K_{j-1}+1}^{K_j} m_i \mathbf{u}_i \Big/ \sum_{i=K_{j-1}+1}^{K_j} m_i \right|. \tag{3}$$

Eq. (3) requires measurement of all velocity components contributing to the mean velocity of the particle group. In order to accurately estimate instantaneous $\mathbf{u}_{\text{meso},j}$, the integral time scale, $T_{\text{integ.}}$, of the values of $m_i\mathbf{u}_i$ should be larger than or equal to Δt_{meso}. $T_{\text{integ.}}$ is here estimated from the autocorrelation function of $q_{P\text{-meso},j}$ (defined below) of the entire time series with $P = m_i|\mathbf{u}_i|$, and from adopting a window shift and a decorrelation scheme to increase frequency resolution (Bergenblock et al., 2006). This autocorrelation describes the correlation between the values of $q_{P\text{-meso},j}$ separated by a time lag, δ times the time interval of the time series Δt_{s} (e.g. $\Delta t_{\text{s}} = \Delta t_{\text{meso}}/10$),

$$c_{qq,\delta} = \sum_{j=0}^{n-\delta-1} (q_{P\text{-meso},j+\delta} - q_{P\text{-meso}})(q_{P\text{-meso},j} - q_{P\text{-meso}}) \tag{4}$$

$c_{qq,\delta}$ normalized by the value at zero time lag $c_{qq,0}$, yields the autocorrelation coefficient

$$C_{qq,\delta} = c_{qq,\delta}/c_{qq,0}. \tag{5}$$

Summation of the normalized autocorrelation function, Eq. (5), until it loses correlation, $T_{\text{c}}/\Delta t_{\text{s}}$ (T_{c} is the correlation time), multiplied by Δt_{s} gives the integral time scale of a time series, $T_{\text{integ.}}$,

$$T_{\text{integ.}} = \Delta t_{\text{s}} \sum_{j=0}^{T_{\text{c}}/\Delta t_{\text{s}}} C_{qq,j+\delta}. \tag{6}$$

First and second order time-moments, $q_{P\text{-meso}}$ and $q'_{P\text{-meso}}$, of an intensive property can be estimated by Eq. (2) as a starting point and then by applying ensemble summation over n particle groups on the corresponding extensive property P of $K_j - K_{j-1}$ particles in each group j within a constant local averaging time Δt_{meso},

$$q_{P\text{-meso}} = \frac{1}{n}\sum_{j=1}^{n} q_{P\text{-meso},j} \approx \frac{1}{n}\sum_{j=1}^{n} \left(\frac{1}{\Delta t_{\text{meso}}|\mathbf{u}_{\text{meso},j}|} \sum_{i=K_{j-1}+1}^{K_j} \frac{P_i}{\rho_{\text{s}} A_{(d,\gamma),i}} \right)_j, \tag{7}$$

$$q'_{P\text{-meso}} = \left[\frac{1}{n}\sum_{j=1}^{n} (q_{P\text{-meso},j} - q_{P\text{-meso}})^2 \right]^{1/2}. \tag{8}$$

In Eq. (7) the particle velocity vector is removed from the summation on the micro level (cf. Eq. (2)) and the occurrence of division by velocities near zero is significantly reduced. In Eq. (7), the time T of Eq. (2) is replaced with $n\Delta t_{\text{meso}}$. The estimation of $q_{P\text{-meso}}$ and $q'_{P\text{-meso}}$ requires that the average length scale of the particle groups $(A_{(d,\gamma),j}|\mathbf{u}_{\text{meso},j}|\Delta t_{\text{meso}})^{1/3}$ should be at least an order of magnitude larger than the average particle diameter of the time series (since particle volume concentration is defined on a length scale much larger than the particle diameter). The selection of Δt_{meso} based on measured $T_{\text{integ.}}$ for the flow will be further discussed in Section 4.

2.2. Time-average probe volume

The time-average size of the measurement probe volume must be derived when applying PDA to unsteady two-phase flow. Fig. 1 shows the geometry of the measurement probe volume inside the entire ellipsoidal probe volume. The cross-sectional area, $A_{(d,\gamma),i}$, introduced in Eqs. (2) and (7), is allowed to vary with particle size, direction of particle path, optical setup, and average measuring conditions. This average area, encountered by particle i, is usually estimated by the classical procedure adopting automatic calibration (Saffman, 1987; Zhang and Ziada, 2000; Albrecht et al., 2003),

$$A_{(d,\gamma),i} = D_{(d,\gamma),i} L_{(d,\gamma),i} \pm \frac{\pi D^2_{(d,\gamma),i}}{4 \sin \Phi} \left| \frac{u_{y,i} \cos \Phi - u_{z,i} \sin \Phi}{|\mathbf{u}_i|} \right|, \tag{9}$$

in which $\mathbf{u}_i = (u_{x,i}, u_{y,i}, u_{z,i})$. In the literature, this conventional procedure has been based on the ensemble average of the measured burst lengths, which may be inappropriate in time-varying flows. The measurement length (z-direction) of the probe volume is truncated by a slit aperture located in the yz-plane with an off-axis angle Φ. $D_{(d,\gamma),i}$ and $L_{(d,\gamma),i}$ are the diameter and the length of the measurement probe volume, projected onto a reference plane normal to the particle trajectory, $e_{\gamma,i}$. The second term on the right-hand side of Eq. (9) represents the projection of the end ellipses onto this reference plane (Zhang and Ziada, 2000). Depending on the signal detection and validation criteria of the PDA processor, this second term should be added or subtracted on the right-hand side of Eq. (9). A reduction of the probe volume due to optically dense conditions is likely to affect both the probe volume's length and diameter.

The reduction in the diameter of the probe volume, due to decreased light intensity (Saffman, 1987), is included in the ensemble average of the burst lengths. However, burst splitting events, which may depend on the residence time of a particle (dependent on velocity) in the measurement volume, require a correction of the 'high-velocity' sampling bias. A correction method is developed in the following, by employing a time-average instead of the conventional ensemble average of the burst lengths.

The cross-section $A_{(d,\gamma),i}$ of Eq. (9), used in Eq. (7), is estimated from the time-average diameter $D_{(d,\gamma),i}$, which in its turn is calculated from the time-average path length $l_{(d,\gamma)}$ of those particles crossing the probe volume that are regarded as valid by the PDA processor. To estimate $D_{(d,\gamma),i}$, the cross-section is usually assumed circular. In this work, the evolution of the cross-section is investigated in detail by calculations based on the generalized Lorenz–Mie theory (Gouesbet et al., 1988). A correction factor, which considers the possible deviation from a circular cross-section, will be introduced in Section 3.3.5. In many cases, the velocity component u_z is not measured, and as described in Section 3.3.3, only particles, which are expected to have $|u_{z,i}/\mathbf{u}_i|$ much smaller than one (particle trajectories in the xy-plane) should be included in the calculation of the time-average diameter of the probe volume associated with particle i. The assumption that a particle has equal probability of crossing any part of the cross-section yields a uniform distribution of particle paths, crossing a reference plane (which passes through the centre of the probe volume normal to $e_{\gamma,i}$). This gives the diameter derived in Appendix A,

$$D_{(d,\gamma),i} = (3\pi/8) l_{(d,\gamma),i}. \tag{10}$$

The precision of $l_{(d,\gamma),i}$ is expected to be rather poor. It is better to estimate this value from a curve-fit of the time-mean values $l_{(d,\gamma),k}$, where each $l_{(d,\gamma),k}$ is obtained from $K_k - K_{k-1}$ particles with diameter d and trajectory angle γ forming Class k:

$$l_{(d,\gamma),k} = \sum_{i_k=K_{k-1}+1}^{K_k} l_{(d,\gamma),i_k} \Delta t_{(d,\gamma),i_k} \Bigg/ \sum_{i_k=K_{k-1}+1}^{K_k} \Delta t_{(d,\gamma),i_k} = \sum_{i_k=K_{k-1}+1}^{K_k} |\mathbf{u}_{(d,\gamma),i_k}| \Delta t^2_{(d,\gamma),i_k} \Bigg/ \sum_{i_k=K_{k-1}+1}^{K_k} \Delta t_{(d,\gamma),i_k}, \tag{11}$$

where index i_k denotes particles sorted according to d and γ. The proposed time-average of the burst lengths, Eqs. (10) and (11), can be used to estimate the size of the cross-sectional area, since it diminishes the effects of Doppler burst splitting, caused by the dependence of the particle residence times on the velocity (a low absolute velocity is statistically related to a long residence time, prone to burst splitting in dense flow, yielding too large particle number density). The effect of burst splitting is reduced when employing Eqs. (10) and (11) to replace the conventional ensemble average (introduced by Saffman, 1987), since in Eq. (11) each length $l_{(d,\gamma),i}$ of a split burst is weighted with its short residence time $\Delta t_{(d,\gamma),i}$ (i.e. not affecting the time-average $l_{(d,\gamma),k}$).

The nominal length of the probe volume is much larger than its nominal diameter and its effective length due to the slit, e.g. Albrecht et al. (2003). So, whereas a strong decay of the intensity of the laser beam may have a significant influence on the diameter of the probe volume, it has a much weaker impact on its effective length. This explains why the effective length of the probe volume is usually considered to be less sensitive to increasing optical thickness. This assumption is obviously not true when there are multiple particles in the probe volume or in its close neighbourhood. However, up to now, there is no known way to consider that

effect. So, in the following, the length of the measurement volume is simply estimated from the imaged slit width l_s,

$$L_{(d,\gamma),i} \approx \left(\frac{l_s}{\sin \Phi}\right)\sqrt{1-\left(\frac{u_{z,i}}{|\mathbf{u}_i|}\right)^2}. \tag{12}$$

3. Experimental setup and procedure

The post-processing algorithm, Eqs. (3)–(12), has been tested experimentally by means of a conventional PDA system (FiberPDA Dantec, 2001) to characterize local particle flow in a riser of a circulating fluidized bed (CFB).

3.1. Circulating fluidized bed

Table 1 presents the operational data of the cold (300 K) fluidized bed, with a cross-section of 0.2×0.2 m^2 and a height of 2.0 m. Spherical glass particles with the polydisperse static size distribution of Fig. 3 were fluidized by air (superficial velocity 0.8 m/s) using a blower at the outlet of the cyclone, see Fig. 4. The volume-weighted median diameter (static) of the particles is 115 μm. The flow was carefully monitored to be symmetric around the centre line in the upper part of the riser; this involved checking that the inlet section and the air distributor did not contain any irregularities. The average particle volume-concentration along the riser's height in the upper region was of the order of 10^{-3} [dimensionless], yielding a rather high optical thickness

Table 1
Circulating fluidized bed and particle characteristics

Parameter	Value
Fluidization velocity	0.8 m s^{-1}
Solids inventory	5.8 kg
Solids recirculation	0.08 kg m^{-2} s^{-1}
Particle properties (average)	
Density (glass)	2400 kg m^{-3}
Refractive index	1.51
Relaxation time	0.064 s
Terminal velocity	0.62 m s^{-1}
Reynolds number	4.5

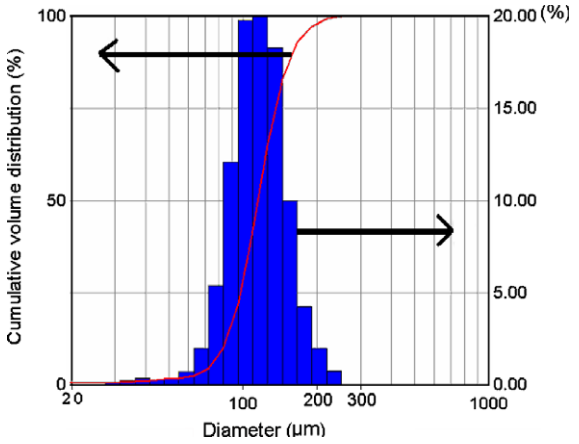

Fig. 3. Static size distribution of fluidized bed particles measured by a laser diffractometer (SprayTech, from Malvern Instruments).

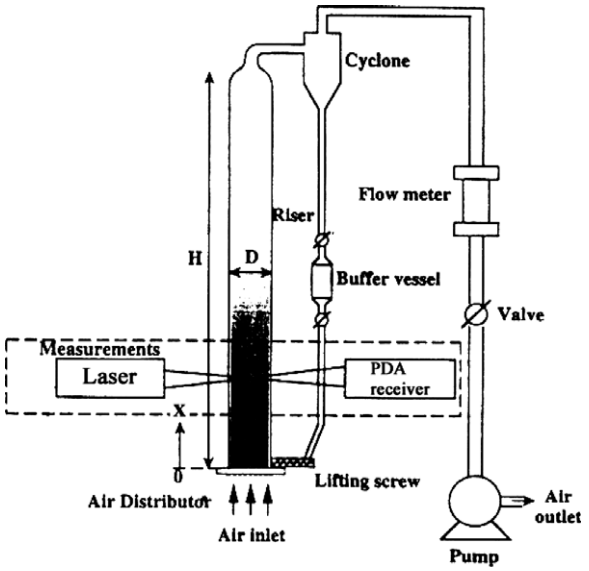

Fig. 4. Schematic drawing of the setup of the cold experimental circulating fluidized bed.

where the PDA measurements were performed. The global time-average mass flux presented in Table 1 was measured by a valve and a buffer vessel in the cyclone leg.

3.2. Optical setup and procedure

The optical setup, the areas/profiles to be measured, and the coordinate system used are all shown in Fig. 5. The conventional PDA system is configured for first order refraction with a Brewster scattering angle to minimize harmful contribution from reflected light. Two velocity components (u_x and u_y, see Figs. 1 and 5) were measured, and hence, u_z was taken to be small compared to $|\mathbf{u}_i|$. The parameters of the optical setup are given in Table 2.

From the measured PDA data, mass flux, particle volume concentration and velocity were estimated. First, however, various issues related to the detection of the particle data are presented, such as measurement errors in particle diameter, Doppler burst splitting, and velocity-filtering to estimate the measurement probe volume. Also, a non-circular extension of the probe volume is considered. Many of these issues related to detection of

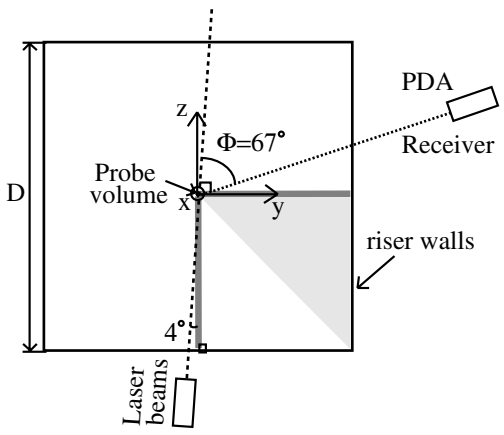

Fig. 5. Sketch of the optical setup. Measurement area and profiles (y and z) are shown in gray.

Table 2
Parameters of the setup of the two-component PDA system manufactured by Dantec Dynamics

Transmitting and receiving optics	
Wavelength of the laser – x	514.5 nm
Wavelength of the laser – y	488.0 nm
Focal lengths	500 mm
Nominal diameter of probe volume – x	149 μm
Nominal diameter of probe volume – y	141 μm
Fringe spacing – x	6.482 μm
Fringe spacing – y	6.148 μm
Receiving optics: 112 mm Fibre PDA	
Off axis angle Φ	67.0°
Aperture	Mask B
Nominal imaged slit width l_s	323 μm

particle data were investigated by means of a global balance of mass flux (which will be described in detail in Section 4.1). In measurement campaigns involving unsteady low-speed flow, covering hundreds of locations in a cross-section of a riser, the length of the time series had to be restricted to in the order of 10000 samples. Such campaigns were performed to estimate time-mean particle volume concentration, velocity and mass flux in the vertical direction at two heights in the riser of the circulating fluidized bed (at $x/H = 0.50$ and 0.75; the average particle volume concentration decreases with height). About 1/8th of the area (see Fig. 5) of the riser's cross-section was covered by 120 measurement points, densely spaced towards the walls (to capture the wall-layers).

3.3. Data processing algorithm

3.3.1. Particle diameter

In the raw PDA time series, about 5% of the diameters were clearly incorrect or not positively validated. The incorrect diameters were outside of the expected size-range (measured with the diffractometer), due to some optical effects like the Gaussian beam or the slit effect (Gréhan et al., 1993). The physical origin of the non-positively validated diameters is difficult to estimate, since the PDA system gives no information on that point. Nevertheless, the origin is probably due to some combined reasons related to the minimum signal-to-noise ratio (SNR) and the improperly denoted "sphericity check" (Albrecht et al., 2003) criteria, which are both connected to complex effects such as laser beams attenuation, multiple scattering, and Gaussian beams effects. These 5% particles should not be excluded in the statistics to evaluate particle volume concentration and mass flux. This is the reason why, in this work, when a diameter was clearly incorrect or not validated, it was assigned the average particle diameter of the correct size measurements derived from the entire time series.

3.3.2. Doppler burst splitting

The measured data were affected by Doppler burst splitting, and a simplified version of the post-processing scheme of van den Moortel et al. (1997) was employed to reduce the effect produced by too large particle number density. The limiting values, identifying burst splitting by a continuity check of succeeding data (e.g. for particle diameter $|d_{i+1} - d_i| < \Delta d$ and $|d_{i+2} - d_i| < \Delta d$, etc.), were chosen by a parametric study, which estimated the global mass flux over the cross-section in the riser from the PDA measurements. These types of continuity check values (e.g. Δd, Δu_x, Δu_y) were introduced by van den Moortel et al. (1997) to correct PDA measurement in optically dense flows. They proved to be valid when estimating global mass flux in the vertical direction of the same riser as used here. All succeeding data, fulfilling the criteria of the continuity check and detected within, say, 0.0040 s, were assumed to originate from burst splitting. The time span 0.0040 s was selected, since the assumed maximum burst length and the minimum velocity were 400 μm and 0.1 m/s, respectively. In this work, less than 10% of the values were lower than this velocity limit (0.1 m/s) because of the vertically directed mean flow and of the high-velocity biased sampling procedure.

Table 3
Mass flux [kg m^{-2} s^{-1}] mapping: A parameter study

Height in riser			$x/H = 0.75$		$x/H = 0.50$	
According to mass balance (measured in cyclone leg)			0.08 ± 0.004		0.08 ± 0.004	
Measured according to commercial PDA system			0.32		0.53	
Evaluated according to present time-mean PDA						
±End ellipses term in Eq. (9)	A+	A−	A+	A−		
Velocity filter coefficients	*Burst split correction*					
$u_f = 2.0$	$\Delta d = 0$ μm	$\Delta u_x = \Delta u_y = 0.00$ m/s	0.100	0.120	0.182	0.219
$u_f = 2.0$	$\Delta d = 5$ μm	$\Delta u_x = \Delta u_y = 0.05$ m/s	0.063	*0.078*	0.108	0.139
$u_f = 2.0$	$\Delta d = 10$ μm	$\Delta u_x = \Delta u_y = 0.10$ m/s	0.050	0.063	0.051	*0.077*
$u_f = 0.1$	$\Delta d = 5$ μm	$\Delta u_x = \Delta u_y = 0.05$ m/s	–	0.143	–	–
$u_f = 3.0$	$\Delta d = 5$ μm	$\Delta u_x = \Delta u_y = 0.05$ m/s	–	0.069	–	–

These split data sampled within 0.0040 s were replaced by their average value at the occurrence of the first split value. The result of the parametric study in Table 3 (to be further explained below) is that the parameters of the continuity check: $\delta d_i < \Delta d$ μm, $\delta u_{x,i} < \Delta u_x$ m/s, $\delta u_{y,i} < \Delta u_y$ m/s (δ means absolute difference between succeeding values and Δ is the limiting value of the variable in the continuity check) should be $\Delta d = 10$ μm, $\Delta u_x = \Delta u_y = 0.10$ m/s at the low ($x/H = 0.50$) and $\Delta d = 5$ μm, $\Delta u_x = \Delta u_y = 0.05$ m/s at the high ($x/H = 0.75$) positions. These correction parameters gave very good agreement between the global time-average mass flux estimated by the PDA over the cross-section at the two heights and the value measured in the cyclone leg (under-predictions of 3.8% at $x/H = 0.50$ and 2.5% at $x/H = 0.75$). Thus, these correction parameters are utilized throughout this work. Note that there is some consistency in the fact that the optimum correction parameters found for the dense case ($x/H = 0.50$) are larger than (here twice) the parameters found for the dilute case ($x/H = 0.75$). In fact, increasing the particle flow density necessarily increases the error on the measured parameters, which require a higher tolerance on the fluctuations (i.e. increase of Δd, Δu_x, Δu_y).

3.3.3. Velocity filtering

The velocity components in the horizontal (u_y) and vertical (u_x) directions were measured. The third (unmeasured) horizontal component (u_z) may not be negligible when estimating the cross-sectional area of the measurement volume, especially in case the absolute value of the vertical component is not much greater than the measured horizontal component. To estimate the diameter of the measurement volume, a velocity filtering is performed; the only data considered were those of particles whose absolute vertical velocity was larger than the maximum measured absolute velocity in the horizontal direction, $|u_{x,i}| > u_f \cdot \max(|u_y|)$ employing a velocity-filter coefficient (u_f). Since only two velocity components were measured, the dependence of the diameter of the measurement volume and area on the particles' trajectory angle is not considered, and the data were binned solely according to particle diameter. The profound effect of the velocity filtering on time-mean vertical mass flux is shown in Table 3, where the velocity-filter coefficient (u_y) was assigned the values 0.1, 2.0 and 3.0. The predicted global mass flux using $u_f = 0.1$ is 0.14 kg m^{-2} s^{-1}. This is twice the result of $u_f = 3.0$, which is only slightly smaller than 0.08 ± 0.004 kg m^{-2} s^{-1} (measured in the cyclone leg) obtained with $u_f = 2.0$. This value ($u_f = 2.0$) yields more data to estimate the probe volume than $u_f = 3.0$ does, and it was used to produce the results of Section 4.

3.3.4. The end ellipses of the cross-sectional area

All the detection and validation criteria of Dantec's PDA system are not accessible to the authors. For instance it is not known, if the term representing the end ellipses in the estimation of the cross-sectional area in Eq. (9) should be added or subtracted. Therefore it was investigated by sensitivity evaluations, whose result is presented in Table 3, as well as in distributions of various flow variables over the cross-section of the riser (not shown). The result favours subtraction of the end-ellipse term (A−) in Eq. (9), since agreement is achieved with the global mass flux measured in the cyclone leg, and subtraction (sign−) was utilized in the following. Note that, this choice of (A−) is also recommended by Albrecht et al. (2003), who argue that particles which

pass through the end ellipses of the volume result in truncated signals that are often not positively validated by the PDA signal processor (Roisman and Tropea, 2001).

3.3.5. Extension of probe volume

A circular effective probe area is assumed in the commonly used estimation procedure of probe area (Saffman, 1987). To find out if the probe area is circular and if the detected light intensity only originates from refracted light (and not from the reflected), the same optical setup was used as in the experiment (except that only the u_x-probe volume was considered) in a calculation of the probe area for a representative selection of particle sizes (eight values). The calculation was based on the generalized Lorenz–Mie theory (Gouesbet et al., 1988; Gréhan et al., 1993). This electromagnetic theory allows the calculation of all the properties of the Doppler signals, produced by a single spherical particle, located at the crossing of two laser beams. It accounts for parameters, such as the waist diameter of the laser beams, polarisation or wavelength, the detectors' position, shape of the aperture and solid angle. The effect of the optical thickness cannot be considered explicitly in the calculation, but it could be accounted for by adjusting the threshold level of the amplitude of the Doppler signal for a small particle (that yields a well-defined circular probe area, based only on refracted light, see below), $d = 25$ μm, so that the calculated mean burst length was equal to the experimental time-mean burst length (extracted from Fig 6, to be further explained below). Fig. 7 shows the result of the Lorenz–Mie calculation in terms of contours of the effective probe area in the xy-plane for the particle diameters, $d = 25$–165 μm. The origin of the y-axis in the figure represents the centre position of the measurement area for $d = 25$ μm. The centre of the probe area moves slightly (in the direction of positive y) with increasing particle size. This movement is not important in this work, since strong spatial gradients in the flow are not present, except very close to the wall (in the wall-layers). It turns out that even at the presently used Brewster scattering angle, there is a reflective scattering mode for medium and large particles, yielding pseudo-elliptical measurement areas, illustrated by the contours in Fig. 7 for y-values below -50 μm. Only for particle diameters below, say, 90 μm, the cross-section of the probe is close to circular. Data of the kind shown in Fig. 7 allow an analytical derivation of the diameter of the probe area under the assumption of a circular cross-section. Therefore this real non-circular (pseudo-elliptical) shape of the probe area can be compared with an equivalent circular description yielding a correction factor: $\xi = A_C/A_D$, where A_C is the correct probe area and A_D is the circular detection area used in the classical expression to estimate the size of the probe volume (see Appendices A and B). $A_D = (\pi/4)D^2$ is estimated in the Lorentz–Mie calculation from the average value ($\langle D\rangle$ – ensemble mean, and $\overline{D}$ – time-mean) of the burst lengths in the x-direction. Fig. 8 shows the estimated correction factors $\langle\xi\rangle$ and $\overline{\xi}$ as a function of particle diameter. A fit of constant values ($\langle\xi\rangle = 1.77$ and $\overline{\xi} = 1.18$) to the calculated correction factors is also shown in the figure. These constant values of the

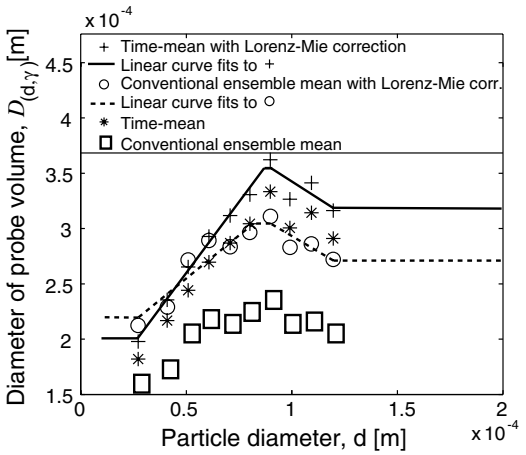

Fig. 6. Diameter of the probe volume, $\langle D_{(d,\gamma),i}\rangle$, as a function of particle diameter (d) for a typical PDA time series measured at the position [x/H, y/D, $z/D = 0.75$; 0; 0].

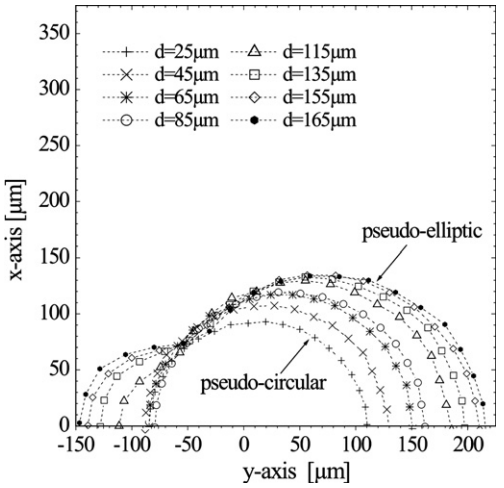

Fig. 7. Contours of the measurement area (A_C) in the xy-plane as a function of particle diameter (d), obtained by the Lorenz–Mie calculation.

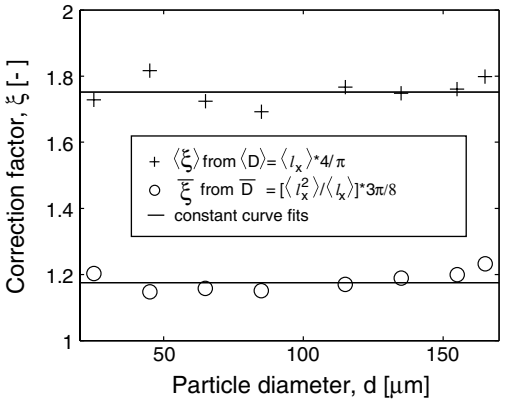

Fig. 8. Ensemble mean, $\langle\zeta\rangle = A_C/\langle A\rangle$ and time mean $\overline{\zeta} = A_C/\overline{A}$ correction factors obtained from Fig. 7 by integration.

correction factor, independent of particle size, were adopted to account for the non-circular evolution of the probe area when generating the results of Table 3 and of Section 4.

3.3.6. Application to time series (500 s)

Two typical time series were selected to investigate the behaviour of the measured raw data (burst lengths) compared to ideal data without any adverse effects due to a high optical thickness, to the presence of one or more particles in the neighbourhood of the probe volume, or to a non-circular evolution of the probe area. Fig. 9 shows cumulative distributions of burst lengths $l_{(d,\gamma),i_k}$ from the two measured time series (500 s), obtained at the centre position of the cross-section of the riser, filtered according to the magnitude of the velocity ($|u_{x,i}| > 2 \cdot \max\{|u_{y,i}|\}$) and binned in the range of $d = 75$–85 μm, yielding 1651 and 3170 samples at $x/H = 0.75$ and 0.50, respectively. Because of the imperfections mentioned in the raw data, the measured curves significantly differ from a corresponding curve for an ideal dilute flow, which is derived in Appendix B under the assumptions of a circular cross-section and no noise. Especially the slopes of the measured and dilute-flow curves deviate for small and large cumulative values, since, in particular, the split of the long burst lengths (which are most likely to split) yields a number of short burst lengths and only a few long ones. It is also shown that the curve associated with the high position ($x/H = 0.75$) is slightly closer to the ideal flow curve than the curve calculated for the low position ($x/H = 0.50$) (the optically denser case). The measured

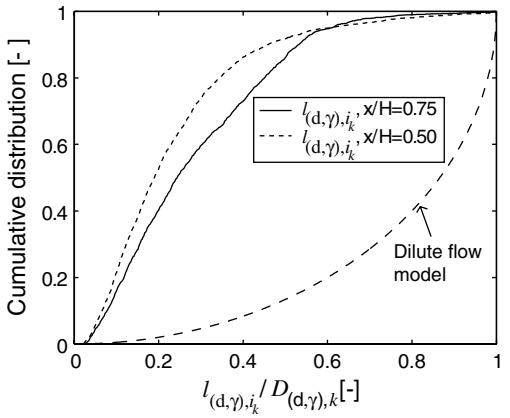

Fig. 9. Cumulative distributions of normalised path lengths $l_{(d,\gamma),i_k}$ (of diameter class k) of two typical measured time series in dense, low-speed two-phase flow, and of a corresponding dilute flow model (Eq. (B4)).

burst lengths will be used to calculate the diameter of the probe volume according to Eq. (10) from the time-mean values of the burst lengths $l_{(d,\gamma),i_k}$ (binned according to particle size) following Eq. (11). The substantial deviation of the measured curves in Fig. 9 from the ideal curve and the impact of burst splitting strongly motivates determination of the probe area (Eq. (9)) based on the averaging suggested, since the time-average better accounts for Doppler burst splitting than the ensemble average. This new time-mean approach will be evaluated against the conventional ensemble average of the burst lengths (Saffman, 1987). These two averaging methods are adopted with and without the correction factors for the non-circular evolution of the probe area, introduced in Section 3.3.5.

Fig. 6 shows the calculated diameter of the probe volume as a function of particle size using the same raw data as input as in Fig. 9 (at $x/H = 0.75$). The results of the present estimation procedure are presented with (+, time mean; ○, ensemble mean) and without (*, time mean; □, ensemble mean) correction for the real (non-circular) extension of the probe volume as a function of particle diameter. The diameter $D_{(d,\gamma),i}$ of the measurement probe volume given by Eq. (10), associated with particle i, is obtained by linear curve fits of the data. Thus, the usual assumption (for the particle size-range used here) that the detected light intensity, scattered by the particle, is proportional to the particle diameter squared is not applied. This is due to the reflective scattering mode, and to the decay of the visibility of the Doppler signals with increasing particles size, as well as to the high optical thickness in the riser. For particles having diameters smaller or larger than the sizes of the valid size bins, constant values are adopted from the ends of the linear curve fits, as shown in Fig. 6. The ensemble mean diameter of the probe volume in Fig. 6, estimated from the burst lengths $l_{(d,\gamma),i_k}$ of Fig. 9 ($x/H = 0.75$), is only 88% of the corresponding time-mean value, 339 μm, due to the remaining effects of Doppler burst splitting. In these cases, the correction for the real extension (non-circular) of the probe volume was used both for the ensemble and time mean values. The conventional ensemble mean diameter (Saffman, 1987), solely based on a circular cross-sectional area, results in a probe diameter that is only 66% of the time-mean value of the non-circular probe diameter, 339 μm. It should also be remembered from Fig. 9 that the effects of burst splitting are strong in the raw data upon which Fig. 6 is based. The raw data consisted of 133% of the number of valid samples. About 28,633 samples were valid and obtained employing the burst split correction scheme. Only 24% of the valid samples were employed to estimate the diameter of the volume of the measurement probe in Fig. 6 owing to the loss of data caused by the velocity filtering and of the incorrectly measured diameters of a few particles. The average of $|u_{y,i}/\mathbf{u}_i|$ is 0.26 of the valid particles, and under the assumption of isotropy for average values of $u_{y,i}$ and $u_{z,i}$, it can be concluded that the unmeasured velocity-component would only have a rather small influence on $A_{(d,\gamma),i}$. Fig. 6 clearly shows that, for large particles ($d > 50$ μm), the conventional ensemble mean (as used in actual PDA systems) underestimates the diameter of the probe volume compared to the (proposed) time-mean method. This discrepancy (underestimation) of the diameter of the probe volume has important consequences for mass flux estimation, which will be shown in Section 4 (Figs. 11 and 12 and Table 4). As mentioned, there is also a difference between the corrected time

Table 4
Comparison between the y- and z-profiles of particle volume concentration, mass flux and velocity of particles in the vertical direction, employing the (proposed) time-mean $\overline{D_{(d,\gamma),i}}$ and the conventional ensemble mean $\langle D_{(d,\gamma),i}\rangle$ to estimate $A_{(d,\gamma),i}$

Height in riser	$x/H = 0.75$							
	Mean (Eq. (7))				RMS (Eq. (8))			
Profile:	y		z		y		z	
Averaging method	$\overline{D_{(d,\gamma),i}}$	$\langle D_{(d,\gamma),i}\rangle$	$\overline{D_{(d,\gamma),i}}$	$\langle D_{(d,\gamma),i}\rangle$	$\overline{D_{(d,\gamma),i}}$	$\langle D_{(d,\gamma),i}\rangle$	$\overline{D_{(d,\gamma),i}}$	$\langle D_{(d,\gamma),i}\rangle$
Vertical mass flux ($kg\,m^{-2}\,s^{-1}$)								
Profile absolute-mean, Eq. (13)	0.21	0.24	0.25	0.29	0.57	0.68	0.58	0.66
Profile-RMS y–z, Eq. (14)	0.08	0.12			0.12	0.19		
Relative diff. y–z, Eqs. (14), (13)	0.39	0.48			0.21	0.27		
Particle volume concentration (–)								
Profile absolute-mean, Eq. (13)	0.0008	0.0009	0.0008	0.0009	0.0015	0.0017	0.0014	0.0016
Profile-RMS y–z, Eq. (14)	0.0002	0.0003			0.0004	0.0006		
Relative diff. y–z, Eqs. (14), (13)	0.26	0.32			0.30	0.34		
Vertical particle velocity ($m\,s^{-1}$)								
Profile absolute-mean, Eq. (13)	0.11	0.11	0.14	0.14	0.16	0.16	0.18	0.18
Profile-RMS y–z, Eq. (14)	0.05	0.05			0.05	0.05		
Relative difference y–z, Eqs. (14), (13)	0.43	0.44			0.31	0.31		
	$x/H = 0.50$							
Vertical mass flux ($kg\,m^{-2}\,s^{-1}$)								
Profile absolute-mean, Eq. (13)	0.73	0.90	0.52	0.59	1.54	2.04	1.11	1.26
Profile-RMS y–z, Eq. (14)	0.28	0.36			0.60	1.00		
Relative differenc y–z, Eqs. (14), (13)	0.39	0.40			0.39	0.49		
Particle volume concentration (–)								
Profile absolute-mean, Eq. (13)	0.0022	0.0029	0.0014	0.0015	0.0030	0.0039	0.0019	0.0020
Profile-RMS y–z, Eq. (14)	0.0011	0.0017			0.0015	0.0023		
Relative difference y–z, Eqs. (14), (13)	0.49	0.58			0.51	0.60		
Vertical particle velocity ($m\,s^{-1}$)								
Profile absolute-mean, Eq. (13)	0.15	0.14	0.15	0.16	0.21	0.22	0.25	0.28
Profile-RMS y–z, Eq. (14)	0.06	0.06			0.06	0.08		
Relative difference y–z, Eqs. (14), (13)	0.41	0.44			0.30	0.36		

mean and the corrected ensemble mean due to the effects of Doppler burst splitting, which the time-mean accounts for.

4. Experimental results and discussion

The general picture of the particle flow in the riser of the CFB with a typical core/wall-layer pattern is in agreement with the results of van den Moortel et al. (1998), obtained by a one-component PDA. Thus, only differences and improvements since that study will be discussed. First, the local averaging time, Δt_{meso} should be chosen. The raw PDA time series (500 s) used to make Figs. 6 and 9 were employed to estimate time-mean, time-RMS, and integral time scale $T_{\text{integ.}}$ of the varying vertical mass flux and velocity of particles in the centre of the cross-section at the two heights (Bergenblock et al., 2006). Fig. 10 shows time moments and integral time scales of mass flux and particle velocity as a function of Δt_{meso}, varied between 0.08 and 0.16 s. At $\Delta t_{\text{meso}} = 0.12$ s, the estimated integral time scales, $T_{\text{integ.}}$, were similar to 0.12 s, and this value was employed in the following predictions, as well as in the generation of Tables 3 and 4. It can also be seen in Fig. 10 that the time-mean estimates do not depend on Δt_{meso}, whereas the time-RMS estimates vary somewhat with Δt_{meso}. The time-RMS estimates decrease with increasing Δt_{meso} for vertical mass flux and they increase with increasing Δt_{meso} for the vertical particle velocity, which is in agreement with the numerical study of Bergenblock et al. (2006).

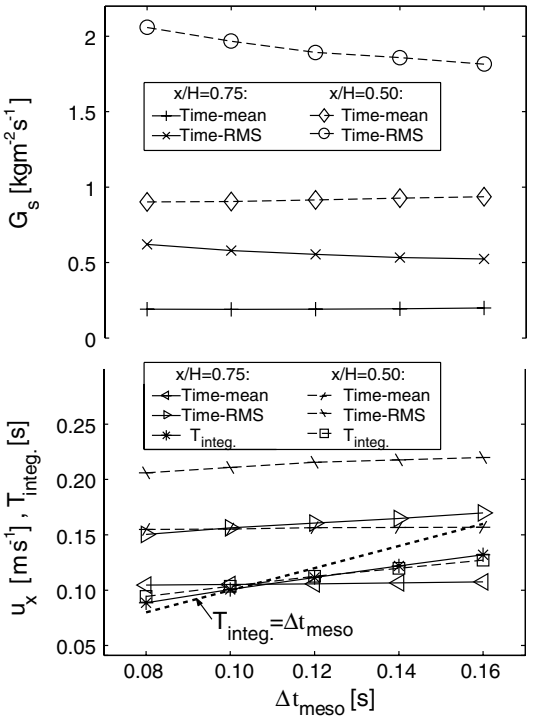

Fig. 10. (a) Fluctuating vertical mass flux, G_s, and (b) particle velocity, u_x, at $y/D = z/D = 0$: time-mean, time-RMS and integral time scales ($T_{\text{integ.}}$) as a function of the local averaging time, Δt_{meso}.

4.1. Time-mean results from two cross-sections

The time-mean (over 60 s) vertical mass flux of the fluidized particles over the entire cross-section was estimated from the processed and valid PDA measurement points by means of an assumption of symmetry in the cross section and a cubic interpolation between the valid estimates to handle scatter in the data in a few positions. The integrated mass flux was compared to the time-average flux measured in the cyclone leg as a validation of the evaluation procedure. The scale in the following figures is quadratic to clearly emphasize the variations in the flow variable. At the height $x/H = 0.75$, the PDA post-processing, shown in Fig. 11, results in a global vertical mass flux of $0.078\ \text{kg m}^{-2}\,\text{s}^{-1}$, which only differs with 2.5% of the value in the cyclone leg ($0.08 \pm 0.004\ \text{kg m}^{-2}\,\text{s}^{-1}$). The integrated PDA value at $x/H = 0.50$ (Fig. 11) ($0.077\ \text{kg m}^{-2}\,\text{s}^{-1}$) differs with 3.8% from the value in the cyclone leg. The corresponding values produced by the commercial PDA system are 0.32 and $0.53\ \text{kg m}^{-2}\,\text{s}^{-1}$ at the high and low positions. Thus, the proposed PDA post-processing, described in Sections 2 and 3, shows a significant improvement compared to the commercial PDA system in this relatively dense, unsteady, two-phase flow.

Particle volume concentrations (c_v) are estimated over the cross-section at the two heights and shown in Fig. 12. At both heights, the distribution of c_v agrees rather well with previous studies; the values are fairly constant and low in the core, whereas they are higher near the walls (in the wall-layers). However, it is somewhat surprising that c_v is lower in the core near the corner of the riser than in its centre. Fig. 13 presents the distributions of the time-mean vertical velocity over the cross-section at the high position $x/H = 0.75$, as well as the conventional ensemble average velocity in the vertical direction. These two velocity distributions deviate significantly; the time-mean velocity is rather uniform in the core as expected, while the ensemble average velocity varies more. The integrated values over the cross-section are very different ($u = 0.08$ and $0.26\ \text{m/s}$), since the estimate of the ensemble average is strongly high-velocity biased due to the sampling procedure and the correlation between density and velocity of particle groups. The proposed time averaging corrects for this type of bias, as well as for the probe volume's dependence on particle size. It should also be noted that the

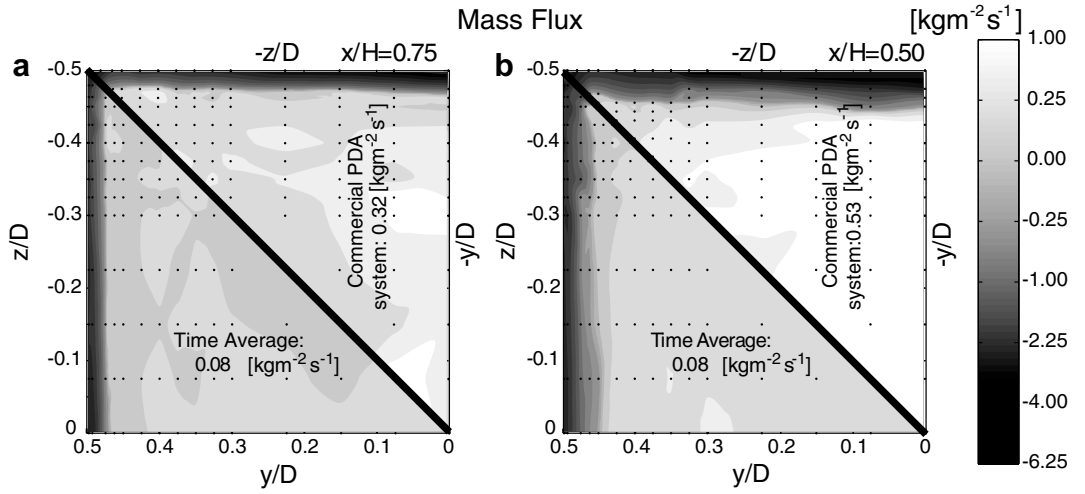

Fig. 11. Vertical mass flux (G_s) for 1/8th of the cross-section: (a) at the high position ($x/H = 0.75$), and (b) at the low position ($x/H = 0.50$) using cubic interpolation between the estimates of the valid measurement points (black dots). Results of the commercial PDA system are shown in the upper right-hand corners and of the proposed processing based on the time average in the lower left-hand corners.

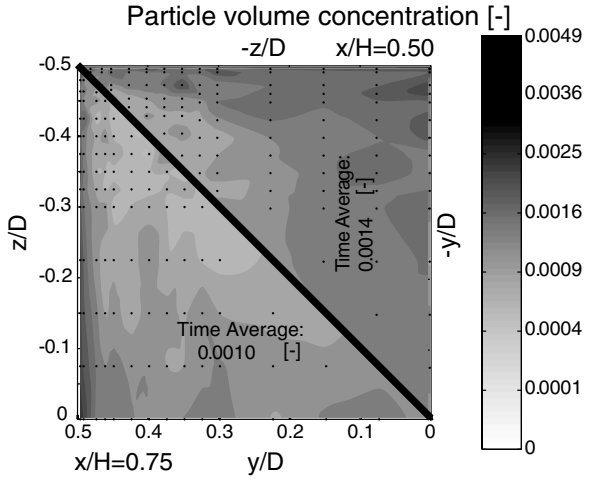

Fig. 12. Particle volume concentration (c_v) for 1/8th of the cross-section at the two heights ($x/H = 0.75$ in the lower left-hand corner, and $x/H = 0.50$ in the upper right-hand corner) using cubic interpolation between the estimates of the valid measurement points (black dots).

integrated time-mean velocity of the particles ($u = 0.08$ m/s) subtracted from the fluidization velocity (0.8 m/s) gives a slip velocity of 0.72 m/s, which is larger than the terminal velocity of an average sized particle (0.62 m/s). This is due to the gravity force and to the fact that the particles are preferentially swept to the lower side of eddies in flows of intermediate Stokes number, such as present in CFB.

4.2. Time-moments for two profiles per height ($x/H = 0.50$ and 0.75)

The profiles of particle-flow variables were compared in the y and z directions in order to evaluate the sensitivity of the results to: (i) the operating conditions of the CFB, to (ii) the probe volume's position in the riser, and to (iii) the effects of the optical thickness. According to the flow structure, with symmetry around the x-axis, these two profiles should be equivalent. Hence, any deviation in the two profiles can be attributed to the PDA measurement.

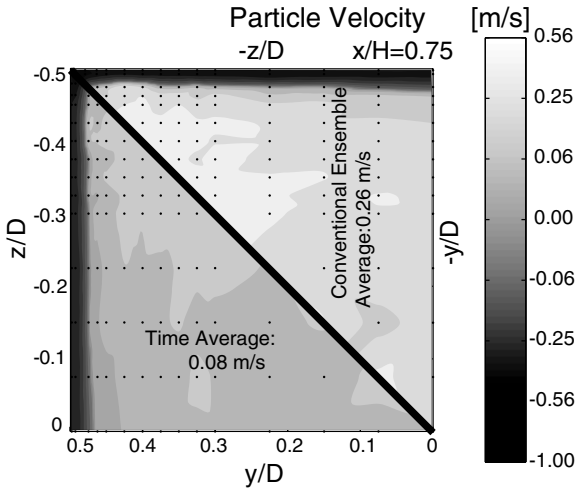

Fig. 13. Vertical velocity (proposed time-average in the lower left-hand corner, and conventional ensemble average in the upper right-hand corner) for 1/8th of the cross-section using cubic interpolation between the estimates of the valid measurement points (black dots).

The variables of the particle flow were calculated from PDA time series of 500 s for the y-profile and of 200 s for the z-profile, Figs. 14 and 15 show time-mean and time-RMS values, respectively, at the two heights as a function of the distance from the nearest wall. The time-average optical thickness between the measurement volume and the wall where the laser beams enter the riser is fairly constant for the y-profile, whereas it varies for the z-profile. From the evaluation of the profiles at the two heights, the conclusion is drawn that, except for a region near the wall where the laser beams enter the riser (distance from wall/$D < 0.2$), yielding large probe volumes due to the high light intensity, the PDA works reasonably well and produces reliable results. The optical thickness reduces the size of the effective measurement volume due to the decreased light intensity. Also, particles in the near neighborhood of the probe volume may strongly perturbate the interference of the laser beams, yielding Doppler burst splitting. The PDA technique was found to perform well when applied to a constant optical thickness (in agreement with the conclusion of van den Moortel et al., 1997) and the estimates in Figs. 14 and 15 of the y- and z-profiles not too close to the wall agree well (say, at a distance from wall/$D > 0.2$). The probe volume of the PDA becomes large near the wall of the laser beams' entry (distance from wall/$D < 0.3$) due to the low optical thickness between the emitter and the measured particle. Consequently, because of the high particle concentration, the probability is high that several particles are present in $V_{(d,\gamma)}$ and/or its close neighborhood, especially during long particle transit times.

In order to quantify the difference between the estimates of the two profiles (y and z), the spatial average of the y profile of the absolute values of a function f_y is calculated as

$$f_{|y|} = \frac{1}{D/2}\int_0^{D/2} |f_{\zeta=y}|\,\mathrm{d}\zeta. \tag{13}$$

For the z profile f_z is calculated accordingly. RMS of the difference between the y and z profiles is expressed as

$$f'_{y-z} = \left[\frac{1}{D/2}\int_0^{D/2} (f_{\zeta=y} - f_{\zeta=z})^2\,\mathrm{d}\zeta\right]^{1/2}. \tag{14}$$

Finally, the relative difference between the two profiles (y and z) is estimated as Eq. (14) divided by Eq. (13) for the y profile, $f'_{y-z}/f_{|y|}$. The reason for dividing by the mean value of the y profile (Eq. (13)) is that the measurements along the y profile are considered more accurate than the z-profile estimates, see Sections 4.2.1 and 4.2.2. Table 4 shows the estimated particle flow variables in terms of the relative difference $f'_{y-z}/f_{|y|}$ of the y and z profiles at the two heights ($x/H = 0.50$ and 0.75) of: (i) the time-averaged values of Figs. 14 and 15 obtained with the diameter of the probe volume $\overline{D_{(d,\gamma),i}}$ according to Eqs. (10),(11), and (ii) the conventional procedure to estimate the size of the measurement volume $\langle D_{(d,\gamma),i}\rangle$ employing an ensemble average of the burst

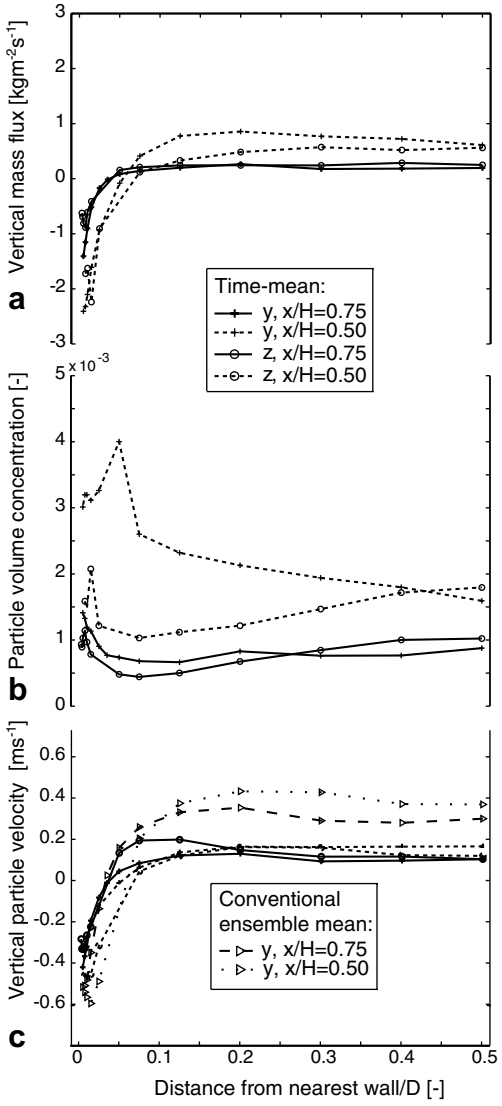

Fig. 14. $y(z=0)$ and $z(y=0)$ profiles of mean values of: (a) estimated particle mass flux (Gs), (b) particle volume concentration (c_v), and (c) particle velocity (u_x), at the high and low positions ($x/H = 0.75$ and 0.50).

lengths (Saffman, 1987). Thus, the only difference between the constructions of the profiles is the averaging used to estimate the size of the measurement volume. These two averaging methods were discussed in Section 3.3 and compared in Fig. 6 (time mean: linear curve fit to +, ensemble mean: linear curve to o).

4.2.1. Estimates of time-mean (Fig. 14 and Table 4)

The time-mean mass fluxes (of the fluidized particles) of the y- and z-profiles are in fairly good agreement ($f'_{y-z}/f_{|y|} = 0.39$ with $\overline{D_{(d,\gamma),i}}$) at both heights. Note that the corresponding values with $\langle D_{(d,\gamma),i}\rangle$ are worse, $f'_{y-z}/f_{|y|} = 0.48$ and 0.40 at the high and low positions, respectively. At the high position, the mass flux profiles are flatter than at the low height, where the profiles are influenced by the dynamics of the splash zone (above the bottom bed). The c_v-estimates (y- and z-profiles) are in very good agreement at the high position ($f'_{y-z}/f_{|y|} = 0.26$), whereas the agreement is not so good ($f'_{y-z}/f_{|y|} = 0.49$) at the low position. This indicates that the effect of the larger optical thickness at the low position, which is experienced by the laser beams and also by the scattered light, adversely affects the accuracy of the results. Again, c_v that is obtained with

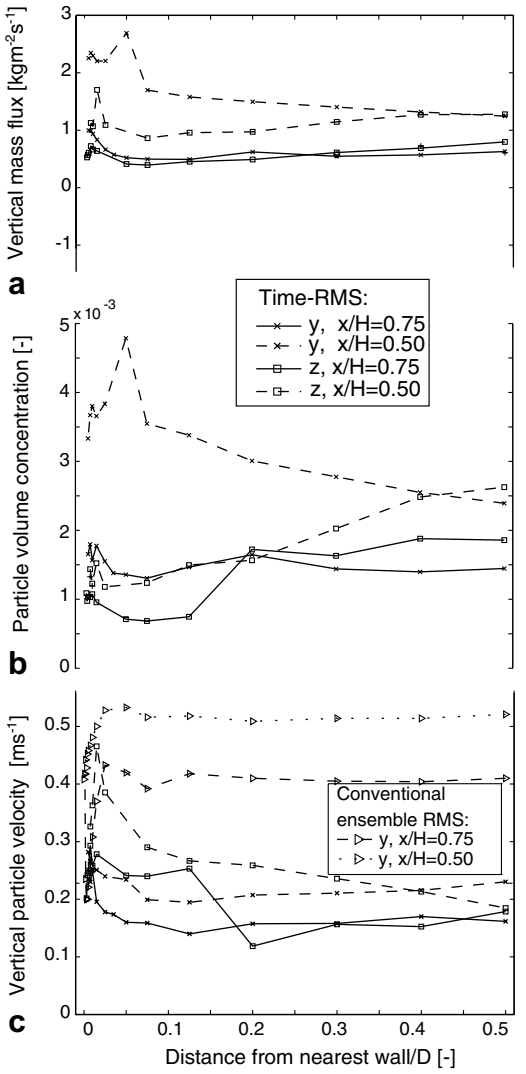

Fig. 15. $y(z=0)$ and $z(y=0)$ profiles of RMS values of: (a) estimated particle mass flux (Gs), (b) particle volume concentration (c_v), and (c) particle velocity (u_x), at the high and low positions ($x/H = 0.75$ and 0.50).

$\langle D_{(d,\gamma),i}\rangle$ are worse $f'_{y-z}/f_{|y|} = 0.32$ and 0.58 (at the high and low positions). In the core of the cross-section, c_v is rather constant at the high position, whereas the estimates at the low position increase towards the wall for the y-profile. The opposite trend is estimated for the z-profile at the low position; c_v decreases towards the wall. This is unexpected and may be explained by the varying optical thickness to which the laser beams are exposed for the z-profile. The average particle concentration is high, especially at the low position. Thus, the probability of the presence of more than one particle in the probe volume or its close neighborhood (yielding Doppler burst splitting) increases towards the wall, since the size of the probe volume increases with reduced optical thickness. The same trend is observed for the estimated time-mean particle velocities; at the high position the y- and z-profiles coincide, except near the wall ($0.05 <$ distance from wall$/D < 0.2$), where the z-profile shows higher velocities than towards the centre of the cross-section. This can be explained by a type of bias of the PDA technique applied to optically dense low-speed flow that has not previously been accounted for (however, its possible existence was recognized by van den Moortel et al. (1997)). High-velocity particles easier become regarded valid than low-speed particles, since high-velocity particles are associated with short average residence time (which are less likely to split than particles with long residence times).

Previously, the result of this bias has been interpreted physically, and regions associated with such bias were shown in figures with local maxima in particle velocities far from the centre of the cross-section (van den Moortel et al., 1998; Mathiesen et al., 2000). This is the case for the conventional ensemble mean values with such maxima at a distance from wall/$D = 0.2$. Also, the huge difference between the time-mean and the conventional ensemble mean of the vertical velocities in the core should be noted. Finally, $f'_{y-z}/f_{|y|} = 0.43$ and 0.41 at the high and low positions, respectively, for the time-mean ($\overline{D_{(d,\gamma),i}}$) of the vertical particle velocities, which indicates that the relative difference between the profile estimates is rather high and similar at the two heights. The corresponding values with $\langle D_{(d,\gamma),i}\rangle$ are high and similar $f'_{y-z}/f_{|y|} = 0.44$ at both heights.

4.2.2. Estimates of time-RMS (Fig. 15 and Table 4)

The estimates of time-RMS values of mass flux (of the fluidized particles), particle volume concentration, and particle velocity represent one of the main novelties of this work. Previously, only ensemble RMS of particle velocities were estimated in unsteady two-phase flow (van den Moortel et al., 1998; Mathiesen et al., 2000), but the ensemble average is high-velocity biased in such flow and therefore unreliable, which is clearly the case when applying ensemble RMS on the present data in Fig. 15c. It can also be seen in the figure that the RMS values of vertical particle velocities decrease with height in agreement with the results of van den Moortel et al. (1998). The estimated time-RMS values of mass flux, particle volume concentration, and particle velocity of Fig. 15 are larger than the corresponding time-mean estimates (see Fig. 14). Clearly, this type of flow can be denoted unsteady (with a statistically steady-state). The time-RMS mass fluxes of the y- and z-profiles (with $\overline{D_{(d,\gamma),i}}$) are in very good agreement at the high position ($f'_{y-z}/f_{|y|} = 0.21$), and in fairly good agreement at the low position ($f'_{y-z}/f_{|y|} = 0.39$). The corresponding values at the high and low positions using $\langle D_{(d,\gamma),i}\rangle$ are worse ($f'_{y-z}/f_{|y|} = 0.27$ and 0.49). At the high and low positions, the time-RMS values of vertical particle velocity and mass flux of the y-profile are rather constant in the core and they increase close to the wall. This type of behavior is expected, since in the wall-layer the particles tend to flow in clusters, which results in large fluctuations. At the low position, the time-RMS of c_v depends on the optical thickness of the medium and the difference between the two profiles has the highest value ($\overline{D_{(d,\gamma),i}} : f'_{y-z}/f_{|y|} = 0.51$ and $\langle D_{(d,\gamma),i}\rangle : f'_{y-z}/f_{|y|} = 0.60$) of all comparisons in Table 4. The time-RMS values of the z-profile show no clear trend; the values are not constant in the core. This can be explained by the varying optical thickness.

5. Conclusions

Phase Doppler anemometry was applied to a dense, unsteady, gas/particle flow (with a statistically steady-state) in the upper part of a circulating fluidized bed. Measures were taken to extend the post-processing algorithm with the purpose of treating low-speed PDA data (vertical and horizontal particle velocities $u_{x,i}$ and $u_{y,i}$, particle residence time Δt_i), particle diameter d_i, and arrival time of the particle t_i. This was accomplished by introducing a local average time Δt_{meso}, which also allows estimates of time-RMS. Measurement campaigns were conducted at two heights ($x/H = 0.50$ and 0.75) in the riser of a laboratory-scale CFB to estimate time-mean and time-RMS values of the following variables of the particle flow: particle volume concentration, mass flux and velocity in the vertical direction. The following conclusions can be drawn:

- The proposed time-average for estimation of the size of the measurement area/volume from the burst lengths better considers the burst splitting events, present in dense flows, than the classical ensemble average. The reason for this is that the residence times of a particle in the measurement volume depends on the velocity; a low absolute particle velocity is often related to a long residence time prone to splitting due to occurrence of one or more particles in the close neighborhood of the probe volume. This new time-average description of the measurement area is more general than the conventional ensemble average by Saffman (1987); hence, the proposed time-average is recommended to be implemented in existing and future PDA processing algorithms.
- Although the present optical setup with a Brewster scattering angle minimizes reflected light, the reflective scattering mode contributed to the effective size of measurement volume for medium and large particles, yielding a non-circular cross-section of the probe area. Therefore, the proposed time-average of the burst lengths was corrected for this non-circular evolution of the measurement volume.

- The previously used ensemble average of the sampled particle velocities is not suitable for estimation of the particle velocity in low-speed unsteady flow, since the PDA data need to be corrected for: (i) sampling bias, related to high velocity and high concentration, and (ii) the varying measurement volume/area. In addition, the velocity must be mass-weighted. The proposed time-mean and time-RMS of variables related to particle flow successfully consider these types of bias.
- The time-mean estimates of the particle flow variables do not depend on the choice of Δt_{meso}, whereas the time-RMS values of vertical mass flux decrease with increasing Δt_{meso}. The opposite is observed for time-RMS of vertical particle velocity and integral time scales (they increase with increasing Δt_{meso}). Δt_{meso} was chosen similar to the integral time scale of fluctuating vertical mass flux.
- In optically dense three-dimensional flow, calibration of the PDA technique may be necessary. Thus, a parametric study of global time-mean mass flux in the vertical direction was performed over the cross-section of the CFB riser at the two heights:
  - The estimated PDA mass fluxes at $x/H = 0.50$ and 0.75 agreed almost exactly (only 3.8% and 2.5% under-prediction) with the time-average value in the cyclone leg ($0.08\ \text{kg m}^{-2}\ \text{s}^{-1}$) after adjusting the continuity-check parameters in particle velocity, diameter, and inter-particle time.
  - A velocity filter $|u_{x,i}| > u_{\text{f}} \cdot \max(|u_{y,i}|)$ was applied to yield only complete particle data to estimate the size of the measurement volume, since only two velocity-components were measured. The constant (u_f) was selected after achieving mass flux agreement between the values of the integrated PDA and the cyclone leg in the parametric study.
- Final estimates along the horizontal y and z profiles:
  - The time-mean of the particle flow variables were successfully estimated and fairly similar at the high position ($f'_{y-z}/f_{|y|} < 0.43$ with $\overline{D_{(d,\gamma),i}}$), fulfilling symmetry, with the exception (especially for particle volume concentration at the low position) in the region (distance from wall/$D < 0.2$) where the laser beams enter the flow. This is so because the optical thickness is low and the average residence time is long, yielding a large probe volume with high risk of simultaneous presence of several particles in the volume of the probe or its neighborhood (missing particles in the flow).
  - The corresponding time-RMS estimates of the y-profile are reliable (especially at the high position) and higher than the time-mean values. The time-RMS estimates are fairly constant in the core and they increase close to the wall. The relative difference between the y and the z profiles is small for vertical mass flux and particle velocity at both heights ($f'_{y-z}/f_{|y|} < 0.39$ with $\overline{D_{(d,\gamma),i}}$), whereas $f'_{y-z}/f_{|y|}$ is high for particle volume concentration at the low position ($f'_{y-z}/f_{|y|} = 0.51$ with $\overline{D_{(d,\gamma),i}}$). This indicates that the average solids volume concentration and optical thickness of the medium at the low height ($x/H = 0.50$) are at the limit where PDA measurements can be reliably performed.
  - The proposed time-average for estimation of the size of the measurement area/volume from the burst lengths is superior to the conventional ensemble average; $f'_{y-z}/f_{|y|}$ (with $\overline{D_{(d,\gamma),i}}$) of vertical mass flux and particle volume concentration are about 20% lower than the corresponding values obtained with $\langle D_{(d,\gamma),i} \rangle$.

Appendix A. Analytical derivation of the diameter of the measurement probe volume

A derivation of the diameter $D_{(d,\gamma)}$ of the measurement probe volume can be made under the assumption of a uniform distribution of particle paths crossing an assumed circular cross-section (with constant $D_{(d,\gamma)}$ of the probe volume at an angle γ). A path length l as a function of the distance y from the centre of the circular cross-section is shown in Fig. A1. In this model only a single particle is considered. Thus, it is referred to as a dilute flow model.

$D_{(d,\gamma),i}$ as a function of $l_{(d,\gamma),i}\Delta t_{(d,\gamma),i}$ in Eq. (11) is derived by shifting from a discrete to a continuous formulation $l_{(d,\gamma),i}\Delta t_{(d,\gamma),i} = l^2/|\mathbf{u}|$, where l is assumed to be independent of $|\mathbf{u}|$. From geometry, l^2 at y is

$$l^2 = D^2 - 4y^2. \tag{A1}$$

The expectation value of l^2 can be written introducing Eq. (A1)

$$E(l^2) = \frac{1}{D}\int_{-D/2}^{D/2}(D^2 - 4y^2)\,\mathrm{d}y = \frac{2}{3}D^2, \tag{A2}$$

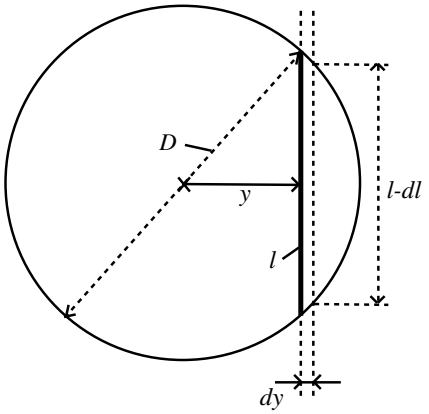

Fig. A1. Geometry of the probe volume for derivation of the expectation values of l and l^2.

and with the substitution of variable $t = \arcsin(2y/D)$, the expectation value of l is

$$E(l) = \frac{1}{D}\int_{-D/2}^{D/2}(D^2 - 4y^2)^{1/2}\,\mathrm{d}y = \frac{D}{2}\int_{-\pi/2}^{\pi/2}\cos^2 t\,\mathrm{d}t = \frac{\pi}{4}D. \tag{A3}$$

For a particle Class k, Eq. (11) can now be written as $E(l^2)/E(l)$, as long as l is independent of $|\mathbf{u}|$,

$$l_{(d,\gamma),k} = \sum_{i_k=1}^{n_k}\frac{l_{(d,\gamma),i_k}^2}{|\mathbf{u}_{(d,\gamma),i_k}|}\Bigg/\sum_{i_k=1}^{n_k}\frac{l_{(d,\gamma),i_k}}{|\mathbf{u}_{(d,\gamma),i_k}|} = \frac{E(l_{(d,\gamma),i_k}^2)E(1/|\mathbf{u}_{(d,\gamma),i_k}|)}{E(l_{(d,\gamma),i_k})E(1/|\mathbf{u}_{(d,\gamma),i_k}|)} = \frac{E(l_{(d,\gamma),i_k}^2)}{E(l_{(d,\gamma),i_k})}, \tag{A4}$$

where n_k should be large enough to statistically represent a uniform distribution. Adopting Eqs. (A2) and (A3) yields

$$E(l_{(d,\gamma),i_k}^2)/E(l_{(d,\gamma),i_k}) = \frac{2}{3}D_{(d,\gamma),k}^2\Big/\frac{\pi}{4}D_{(d,\gamma),k}, \tag{A5}$$

and finally the time-average diameter of the probe volume is, in agreement with Eq. (10),

$$D_{(d,\gamma),k} = \left(\frac{3\pi}{8}\right)l_{(d,\gamma),k} \approx 1.19\,l_{(d,\gamma),k}. \tag{A6}$$

Appendix B. Derivation of the cumulative PDF of path lengths

An analytical derivation of the probability density function (PDF) of path lengths passing a circular cross-section with a uniform distribution along the y-axis in Fig. A1 was given by Fandrey et al. (2000). Here, this PDF $P(l)$ is employed to derive a cumulative PDF, which corresponds to $y(l)$. $P(l)$ was derived, after differentiating Eq. (A1), yielding

$$P(l) = \left|\frac{\mathrm{d}y}{\mathrm{d}l}\right| = \frac{1}{2}\,l(D_{(d,\gamma)}^2 - l^2)^{-1/2}, \tag{B1}$$

and if $P(l)$ is integrated between 0 and $D_{(d,\gamma)}$, the maximum cumulative value is

$$\begin{aligned}\int_{l=0}^{l=D_{(d,\gamma)}} P(l)\,\mathrm{d}l &= \left[\begin{array}{c} -l^2 = t \\ l\,\mathrm{d}l = -1/2\,\mathrm{d}t\end{array}\right] = \frac{1}{2}\int -\frac{1}{2}(D_{(d,\gamma)}^2 + t)^{-1/2}\,\mathrm{d}t = \left[-\frac{1}{2}(D_{(d,\gamma)}^2 + t)^{1/2}\right] \\ &= \left[-\frac{1}{2}(D_{(d,\gamma)}^2 - l^2)^{1/2}\right]_{l=0}^{l=D_{(d,\gamma)}} = \frac{1}{2}D_{(d,\gamma)},\end{aligned} \tag{B2}$$

which correctly agrees with the maximum value of y.

Dividing Eq. (B1) by Eq. (B2) gives the normalized PDF

$$P(l)/\frac{1}{2}D_{(d,\gamma)} = \frac{l}{D_{(d,\gamma)}}\left(D_{(d,\gamma)}^2 - l^2\right)^{-1/2}. \tag{B3}$$

Integration of the normalized PDF gives the cumulative PDF

$$\begin{aligned}\int_{l=0}^{l} \frac{l}{D_{(d,\gamma)}}\left(D_{(d,\gamma)}^2 - l^2\right)^{-1/2}\mathrm{d}l &= \left[\begin{array}{c} -l^2 = t \\ l\,\mathrm{d}l = -1/2\,\mathrm{d}t \end{array}\right] = -\frac{1}{2D_{(d,\gamma)}}\int \left(D_{(d,\gamma)}^2 + t\right)^{-1/2}\mathrm{d}t \\ &= \left[-\frac{1}{D_{(d,\gamma)}}\left(D_{(d,\gamma)}^2 - l^2\right)^{1/2}\right]_{l=0}^{l} = 1 - \left(1 - \frac{l^2}{D_{(d,\gamma)}^2}\right)^{1/2}. \end{aligned} \tag{B4}$$

References

Albrecht, H.E., Damaschke, N., Borys, M., Tropea, C., 2003. Laser Doppler and Phase Doppler Measurement Techniques. Springer, Berlin.

Bergenblock, T., Leckner, B., Onofri, F., Occelli, F., Tadrist, L., 2006. Averaging of particle data from phase Doppler anemometry in unsteady two-phase flow: Validation by numerical simulation. Int. J. Multiphase Flow 32, 248–268.

Berkelmann, K.G., Renz, U., 1991. Gas and solid flow in the freeboard of a fluidized-bed combustor. Powder Technol. 68, 271–280.

Buchhave, P., George, W.K., Lumley, J.L., 1979. The measurement of turbulence with the laser-Doppler anemometer. Ann. Rev. Fluid Mech. 11, 443–503.

Dantec A/S, 2001. Software BSA v2.12 SP4.

Edwards, C.F., Marx, K.D., 1992. Analysis of the ideal phase-Doppler system: limitations imposed by the single-particle constraint. Atomization Spray. 2, 319–366.

Fandrey, C., Naqwi, A., Shakal, J., Zhang, H., 2000. A phase Doppler system for high concentration sprays. In: Proceedings of the 10th International Symposium on Applications of Laser Techniques to Fluid Mechanics, Paper 20.3, Lisbon, July 10–13.

Gouesbet, G., Maheu, B., Gréhan, G., 1988. Light scattering from a sphere arbitrarily located in a Gaussian beam, using a Bromwich formulation. J. Opt. Soc. Am. A 9, 1427–1443.

Gréhan, G., Gouesbet, G., Naqwi, A., Durst, F., 1993. Particle trajectory effects in phase Doppler systems: computations and experiments. Part. Part. Syst. Char. 10, 332–338.

Hamdullahpur, F., Mackay, G.D.M., 1986. 2-Phase flow behavior in the freeboard of a gas-fluidized bed. AICHE J. 32, 2047–2055.

Hardalupas, Y., Horender, S., 2001. Phase Doppler anemometer for measurements of deterministic spray unsteadiness. Part. Part. Syst. Char. 18, 205–215.

Ibsen, C.H., Solberg, T., Hjertager, B.H., 2001. Evaluation of a three-dimensional numerical model of a scaled circulating fluidized bed. Ind. Eng. Chem. Res. 40, 5081–5086.

Ibsen, C.H., Helland, E., Hjertager, B.H., Solberg, T., Tadrist, L., Occelli, R., 2004. Comparison of multifluid and discrete particle modelling in numerical predictions of gas particle flow in circulating fluidised beds. Powder Technol. 149, 29–41.

Levy, Y., Lockwood, F.C., 1983. Laser Doppler measurements of flow in freeboard of a fluidized-bed. AICHE J. 29, 889–895.

Mathiesen, V., Solberg, T., Hjertager, B.H., 2000. An experimental and computational study of multiphase flow behavior in a circulating fluidized bed. Int. J. Multiphase Flow 26, 387–419.

McLaughlin, D.K., Tiederman, W.G., 1973. Biasing correction for individual realization of laser anemometer measurements in turbulent flows. Phys. Fluids 16, 2082–2088.

Onofri, F., Bergougnoux, L., Firpo, J-L., Mesguish-Ripault, J., 1999. Velocity, size and concentration measurements of optically inhomogeneous cylindrical and spherical particles. Appl. Opt. 38, 4681–4690.

Roisman, I.V., Tropea, C., 2001. Flux measurements in sprays using phase Doppler techniques. Atomization Spray. 11, 667–669.

Saffman, M., 1987. Automatic calibration of LDA measurement volume size. Appl. Opt. 26, 2592–2597.

Samuelsberg, A., Hjertager, B.H., 1996. An experimental and numerical study of flow patterns in a circulating fluidized bed reactor. Int. J. Multiphase Flow 22, 575–591.

Sankar, S.V., Inenaga, A., Bachalo, W.D., 1992. Trajectory dependent scattering in Phase Doppler interferometry: minimizing and eliminating sizing error. In: Proceedings of the 6th International Symposium on Applications of Laser Techniques to Fluid Mechanics, Paper 12.2, Lisbon.

van den Moortel, T., Santini, R., Tadrist, L., Pantaloni, J., 1997. Experimental study of the particle flow in a circulating fluidized bed using a phase Doppler particle analyser: a new post-processing data algorithm. Int. J. Multiphase Flow 23, 1189–1209.

van den Moortel, T., Azario, E., Santini, R., Tadrist, L., 1998. Experimental analysis of the gas-particle flow in a circulating fluidized bed using a phase Doppler particle analyzer. Chem. Eng. Sci. 53, 1883–1899.

van de Wall, R.E., Soo, S.L., 1994. Measurement of particle cloud density and velocity using laser devices. Powder Technol. 81, 269–278.

Wang, T., Lin, Z.J., Zhu, C.M., Liu, D.C., Saxena, S.C., 1993. Particle-velocity measurements in a circulating fluidized-bed. AICHE J. 39, 1406–1410.

Werther, J., Hage, B., Rudnick, C., 1996. A comparison of laser Doppler and single-fibre reflection probes for the measurement of the velocity of solids in a gas–solid circulating fluidized bed. Chem. Eng. Process. 35, 381–391.

Yang, Y.L., Jin, Y., Yu, Z.Q., Wang, Z.W., 1992. Investigation on slip velocity distributions in the riser of dilute circulating fluidized-bed. Powder Technol. 73, 67–73.

Zhang, Y.F., Arastoopour, H., 1995. Dilute fluidized cracking catalyst particles – gas-flow behavior in the riser of a circulating fluidized-bed. Powder Technol. 84, 221–229.

Zhang, Zh., Ziada, S., 2000. PDA measurements of droplet size and mass flux in the three-dimensional atomisation region of water jet in air cross-flow. Exp. Fluids 28, 29–35.